processes

MDPI

Article

Bi-Functional Catalyst/Sorbent for a H_2-Rich Gas from Biomass Gasification

Francesca Micheli [1,2], Enrica Mattucci [2], Claire Courson [1,*] and Katia Gallucci [2]

[1] Institut de Chimie et Procédés pour l'Énergie, l'Environnement et la Santé, UMR CNRS 7515, ECPM, University of Strasbourg, 25 rue Becquerel, CEDEX 2, 67087 Strasbourg, France; francesca.micheli@hotmail.com

[2] Department of Industrial Engineering, University of L'Aquila, Monteluco di Roio, 67100 L'Aquila, Italy; enricamattucci@gmail.com (E.M.); katia.gallucci@univaq.it (K.G.)

* Correspondence: claire.courson@unistra.fr; Tel.: +33-368-852-770

Abstract: The aim of this work is to identify the effect of the CaO phase as a CO_2 sorbent and mayenite ($Ca_{12}Al_{14}O_{33}$) as a stabilizing phase in a bi-functional material for CO_2 capture in biomass syngas conditioning and cleaning at high temperature. The effect of different CaO weight contents is studied (0, 56, 85, 100 wt%) in sorbents synthesized by the wet mixing method. These high temperature solid sorbents are upgraded to bi-functional compounds by the addition of 3 or 6 wt% of nickel chosen as the metal active phase. N_2 adsorption, X-ray diffraction, scanning electronic microscopy, temperature-programmed reduction analyses and CO_2 sorption study were performed to characterize structural, textural, reducibility and sorption properties of bi-functional materials. Finally, sorption-enhanced reforming of toluene (chosen as tar model), of methane then of methane and toluene with bi-functional compounds were performed to study the best material to improve H_2 content in a syngas, provided by steam biomass gasification. If the catalytic activity on the sorption enhanced reforming of methane exhibits a fast fall-down after 10–15 min of experimental test, the reforming of toluene reaches a constant conversion of 99.9% by using bi-functional materials.

Keywords: tar removal; hydrogen production; CO_2 capture; bi-functional materials; Ni-based catalyst; CaO sorbent

Citation: Micheli, F.; Mattucci, E.; Courson, C.; Gallucci, K. Bi-Functional Catalyst/Sorbent for a H_2-Rich Gas from Biomass Gasification. *Processes* **2021**, *9*, 1249. https://doi.org/10.3390/pr9071249

Academic Editor: Albert Ratner

Received: 29 June 2021
Accepted: 14 July 2021
Published: 19 July 2021

1. Introduction

Depending on the degree of integration in the combustion/gasification plants, there are intrinsic benefits to gain from the utilization of CO_2 separation: at atmospheric pressure, the required heat for high-temperature calcination (over 900 °C) is recovered from the exothermic carbonation reaction taking place at 650 °C working as a thermal flywheel. When CO_2 capture is performed contemporary to the hydrocarbon reforming, the exothermic heat released by the carbonation reaction (2) can be used to run the endothermic hydrocarbon steam reforming reaction (1):

$$C_nH_m + 2_nH_2O \rightleftarrows nCO_2 + (m/2+2n)\ H_2 \quad (1)$$

$$MO + CO_2 \rightleftarrows MCO_3\ (M = \text{alkaline metal}) \quad (2)$$

In sorption enhanced reaction processes (SERP) or sorption-enhanced water–gas shift (SEWGS), the carbonated sorbent, preventing CO_2 accumulation in the gas phase, drives the equilibrium of the reaction towards H_2 production according to Le Chatelier's principle.

In order to work properly, a sorbent must have several properties [1], such as high sorption working capacity, high selectivity for carbon dioxide, fast sorption/desorption kinetics, stable sorption/desorption capacity after repeated cycles, regeneration without extreme pressure or temperature conditions, adequate mechanical strength of sorbent particles and tolerance to the presence of water or impurities.

The use of CaO-based solids to capture CO_2 at a high temperature (>500 °C) is the core of several Carbon Capture and Storage (CCS) techniques and zero emission power plant concepts. These technologies utilize the concept of reversible reaction between CaO and CO_2 to form calcium carbonate (reaction (2)) in a calcium looping cycle under Temperature Swing Adsorption (TSA) conditions.

Although CaO presents some limitations in the temperature range of WGS interest [2–4], it has been proven to be an advantageous sorbent in the field of pre-combustion processes [5], chemical looping [6,7] and sorption enhanced hydrocarbon reforming [8–14].

Promising materials based on the use of inert support (as mayenite) can avoid the sintering problems due to high regeneration temperature during CO_2 multicycle sorption/desorption [15,16] ensuring a better efficiency than dolomite or limestone [17]. This type of Ca-based sorbent was potentially interesting for high temperature applications when combined with a transition metal to produce bi-functional materials for activity in steam methane and toluene reforming [13,18–20].

Martavaltzi et al. [21] synthesized CaO on mayenite ($Ca_{12}Al_{14}O_{33}$) following the synthesis method reported by Li et al. [15]. The increase in the mixing time and aging generated bigger crystals that reduced specific surface area, hence CO_2 uptake. Water addition before the second calcination step increased sorption capacity due to the formation of a uniform porous network and higher pore volume. Calcination temperature above 1000 °C leads to the formation of $Ca_3Al_2O_6$, bringing the decline of CO_2 uptake and moreover, sintering the sorbent before high-temperature regeneration [17].

Several authors have studied the CaO to mayenite ratio indicating an optimal range of values between 75/25 and 85/15 [21–23]. The sorption behavior of a material containing 75–85 wt% of CaO on mayenite prolonged carbonation prior to the cycling tests and the hydration step during synthesis improved the stability of the uptake capacity [24]. The sorbent with 75 wt% of CaO kept good stability up to the 150th cycle under severe conditions (regeneration at 1000 °C under 86 vol% of CO_2).

Various synthesis methods (as wet chemistry, sol-gel, and decomposition) or pre-treatments (as hydration or prolonged carbonation) were evaluated. The method optimized by Zamboni [13] was chosen to study their performance similarities with a variation of CaO precursor and CaO amount.

Many authors have investigated the choice of the best CaO precursor for CO_2 uptake. Lu et al. [25] screened two different precursors: $Ca(OH)_2$ and $Ca(COOCH_3)_2$ without finding any difference in morphology and textural properties, but in CO_2 uptake, the sorbent derived from the $Ca(COOCH_3)_2$ precursor results in a higher sorption capacity. Various calcium salts calcined at 900 °C for 30 min were tested in TGA sorption cycles [26]; CaO derived from calcium acetate and calcium D-gluconate have the highest capacities and decay resistances, with similar initial conversions.

In terms of SESR, bi-functional materials are still of interest [27]. In the SESR of methane and toluene (as tar model compound), Ni is the most studied transition metal because it can be efficient from low content (3 wt%) in the bi-functional materials [28] and remains cheaper than noble metals, even in a lower concentration. In fact, larger contents of Ni typically lead to coke formation [29].

The aim of this work is to synthesize solid sorbents for CO_2 capture for the best biomass syngas conditioning and cleaning, in particular:

- for an efficient abatement of unwanted and harmful heavy hydrocarbons (known as tar) produced during the gasification process
- for reforming of methane at low temperature (640–650 °C) with low Ni content to avoid its sintering
- and, finally, for an almost pure H_2 in the syngas.

CaO based materials with $Ca(COOCH_3)_2$ chosen as the CaO precursor were synthesized as a CO_2 sorbent for high-temperature application. These high temperature solid sorbents were upgraded to bi-functional compounds for simultaneous CO_2 sorption and

steam methane and tar reforming, also called sorption enhanced reforming. The transition metal (Ni) was added by impregnation technique.

Characterization techniques such as N_2 adsorption (BET and BJH), X-ray diffraction (XRD), scanning electronic microscopy (SEM), temperature-programmed reduction (TPR) and CO_2 sorption study were performed to characterize structural, textural and sorption properties of bi-functional materials. Finally, sorption enhanced reforming of toluene as a tar model compound (SERT), sorption enhanced reforming of methane (SERM) then sorption enhanced reforming of methane and toluene (SERMT) with bi-functional compounds were studied to select the better material improving H_2 content in a syngas provided by steam biomass gasification.

2. Materials and Methods

2.1. Synthesis

$CaO/Ca_{12}Al_{14}O_{33}$ systems were synthesized as high temperature solid sorbents, then upgraded to bi-functional compounds with different Ni contents.

2.1.1. Sorbents Synthesis

In order to optimize the sorption process and its stability, a method to vary the $CaO/Ca_{12}Al_{14}O_{33}$ mass ratio was used to synthesize the $CaO\text{-}Ca_{12}Al_{14}O_{33}$ phases. This synthesis is based on the method firstly reported by Li et al. [21] and modified by Zamboni et al. [13] to increase the mechanical stability of the sorbent and uses $Ca(C_2H_3O_2)_2$ as a calcium precursor. The sorption process is optimized choosing high $CaO/Ca_{12}Al_{14}O_{33}$ mass ratios (85/15 and 56/44 noted C85 and C56, respectively) and the stability of the catalyst is investigated with mayenite alone (0/100, noted May).

For comparison, the CaO sorbent (noted C100) was prepared from calcium acetate calcination at 750 °C for 4 h with a temperature ramp of 3 °C min^{-1}.

2.1.2. Synthesis of Bi-Functional Materials

For the synthesis of bi-functional materials, 3 or 6 wt% of Ni is added by impregnation. Nickel nitrate hexahydrate ($Ni(NO_3)_2$ $6H_2O$) is dissolved in water. Temperature is fixed at 70 °C (for complete solubilization and the best dispersion) and the impregnation process of the solid sorbents lasts for 1 h. The remaining water is evaporated in an oven at 120 °C for 12 h.

Finally, the bi-functional compound is thermally treated to enhance the transformation of the metallic precursor to the corresponding oxide and its metal/support interactions. This last step can change the specific surface area, the porosity and the metal dispersion on the support surface, but also the mechanical resistance. The calcination is performed at 900 °C for 4 h with a temperature ramp of 3 °C min^{-1} and leads to the bi-functional materials named C100Ni3, C56Ni3, and MayNi3 containing 3 wt% of Ni and C100Ni6, C56Ni6, MayNi6 containing 6 wt% of Ni on various sorbents (C100, C56, and May, respectively).

2.2. Characterization

2.2.1. BET/BJH

Brunauer–Emmett–Teller and Barrett–Joiner–Halenda (BET and BJH) analytical methods are used to determine the surface properties (specific surface area, pore volume and pore size) of the samples (degassed under vacuum at 5 mmHg min^{-1} and 200 °C during 4–5 h) by N_2 physisorption at 77 K using a Micrometrics ASAP 2000.

2.2.2. XRD

X-ray diffraction (XRD) gives information about crystal phases present in samples and their crystallite size by the Scherrer formula [30], evaluated from the half-high length of the principal and best deconvolved diffracted ray. The sample is prepared as a powder (<100 μm).

The used diffractometer is a diffractometer BRUKER D8 Advance equipped with a copper anti-cathode (Kα = 1.5418 Å). The diffracted rays' intensity is measured by a LynxEye detector. The database used for the crystal phases fitting is the ICSD (Inorganic Crystal Structure Database).

2.2.3. SEM

Particle morphology of the samples is observed by SEM images obtained by a Philips XL30 CP. To identify the elemental composition, the energy-dispersive X-ray spectroscopy (EDS) technique is coupled. Samples in the form of powder are sticked on a cylindrical sample carrier and observed on their external surface.

2.2.4. Temperature-Programmed Reduction

Temperature-programmed reduction (TPR) technique is used to evaluate the temperature range to realize the reduction of the catalytic oxide, leading to the knowledge of the interaction between the support and the active phase, and the reducibility percentage of metallic oxides.

The analyses are carried out in Micromeritics Autochem chemisorption equipment. The reducibility of sorbents/catalysts under hydrogen is carried out on 50–100 mg of material.

Firstly, decomposition of possible carbonates is performed from room temperature to 900 °C under argon atmosphere; secondly, the reductive gas mixture (10 vol% of H_2 in Ar) flowed through the reactor heated from room temperature to 1000 °C with a slope of 15 °C min^{-1} and is maintained at 1000 °C for 30 min. A thermal conductivity detector (TCD) allows the quantitative determination of hydrogen consumption until return to the baseline.

2.3. Sorption Tests (TGA)

CO_2 sorption capacity and sorption cyclic behaviour of the synthesized samples are evaluated at atmospheric pressure using the thermo-balance TGA Q5000 IR of TA Instruments.

Moisture and CO_2 present on samples are previously removed (regeneration step) under He flow and at high temperature (800 °C). The sorption phase is performed at 650 °C for 30 min after a heating ramp of 10 °C min^{-1} and takes place under 10 vol% CO_2-He mixture. The number of cycles varied from 10 to 30.

2.4. Reactivity Tests

2.4.1. Sorption Enhanced Reforming of Toluene

In the first approach, toluene has been considered as a tar model compound for catalytic steam reforming tests [31]. A stoichiometric amount of water considering also the WGS reaction has been used according to the reaction (3), hence the steam to carbon molar ratio (S/C) is fixed equal to 2.

$$C_7H_8 + 14\,H_2O \rightarrow 7\,CO_2 + 18\,H_2 \quad (3)$$

At the same time, CaO carbonation takes place according to the reaction (4):

$$CaO + CO_2 \rightarrow CaCO_3 \quad (4)$$

The WHST (Weight Hourly Space Time) has been fixed to 0.0166 g_{cat} h Nl^{-1}. Toluene concentration (5 g Nm^{-3}) was chosen to perform catalytic tests in conditions similar to those observed in the syngas composition at the exiting biomass fluidized bed gasifier (about 2 to 10 g Nm^{-3}) [32].

Catalytic activity in steam toluene reforming is evaluated at 640 °C in a fixed bed reactor. The experimental setup (Figure 1) is composed of a fixed bed quartz reactor (inner diameter 8 mm) containing a sorbent/catalyst bed in a 10 mm height (100 mg),

supported by quartz wool and placed in a furnace in which the heating is monitored by a thermocouple adherent to the reactor bed wall. The top of the sample bed is charged with 100 mm of quartz chips to assure proper mixing of all the reagents. Using two HPLC pumps, water and toluene are introduced into a vaporization furnace (250 °C), and then carried to the reactor by a flow (total flow of 50 Nml min^{-1}) containing a mixture of argon (carrier gas) and nitrogen (internal standard) through electrically heated lines to avoid vapor condensation. A second line allows for sending purge gas (Ar) or other gas such as H_2 to pre-reduce the catalyst before a test, if needed. At the exit of the reactor, reaction products are continuously injected in three different chromatographs: Varian star 3400CX with FID (flame ionization detector) analyzer to quantify heavy molecules such as toluene, benzene and the other heavy hydrocarbons; Delsi Instruments Di200 and Agilent 7890A with TCD detectors have been used to detect CO_2, H_2, CO, CH_4 and N_2. Every catalyst has been tested for 230 min under constant operative conditions; catalysts are not pre-reduced, because the reduction takes place in situ.

2.4.2. Sorption Enhanced Reforming of Methane

Catalytic activity in steam methane reforming is evaluated in the experimental setup previously used for steam toluene reforming tests (Figure 1).

Every catalyst (100 mg) was pre-reduced before each test under a mixture of Ar/H_2 (10 vol% of H_2): a flow rate of 50 Nml min^{-1} is feed to the reactor and temperature is risen up to the set point temperature of 850 °C with a rate of 3 °C min^{-1}; thereafter, an isotherm is kept for 1 h and 30 min.

The reactive feed mixture is composed of 56.8 vol% of N_2, 33.2 vol% of steam, and 10.0 vol% of CH_4. In Table 1, the operating conditions used during catalytic tests are reported.

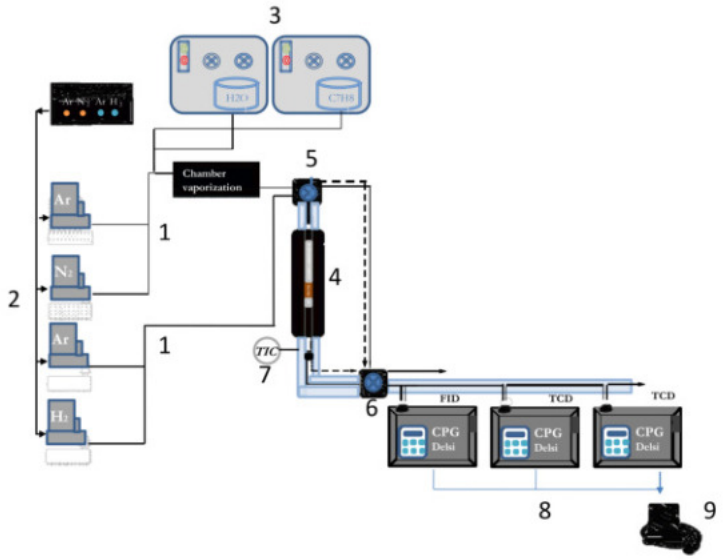

Figure 1. Experimental setup: 1: gas lines; 2: mass flow controllers; 3: water and toluene HPLC pumps; 4: furnace and reactor; 5–6: six-ways valves; 7: thermocouple; 8: chromatographs; 9: computer.

Table 1. Operating conditions of steam methane reforming tests.

Operating Parameters	Set Point
Temperature (°C)	640
Pressure (atm)	1
Total flow rate (ml min^{-1}) at 25 °C	10
H_2O/CH_4 molar ratio	3
WHST (g_{cat} h Nl^{-1})	0.17
Ni-WHST (g_{cat} h Nl^{-1})	0.005

2.4.3. Sorption Enhanced Reforming of Methane and Toluene at Higher WHST

The SERMT plant is conceptually similar to the bench scale of the SETR and SEMR [33,34]. Gaseous phases are sent to the system by mass flow controllers. Liquid water and toluene are fed by KDS Legato 100 syringe pumps, vaporized into the evaporator and mixed with the inlet gas flow. The gas/steam mixture reaches the micro-reactor, placed in an electrical furnace, set at 650 °C after the pre-reduction step. The material (9 g) is packed in the micro-reactor (OD = 10 mm) between inert sand layers (d_p = 850–1000 µm). A cooling zone follows the furnace; it also contains a condenser to collect unreacted water and toluene during tests. Two pressure indicators are installed to monitor the pressure drop during the test. Exiting gas is sent to the InfraRed analyzer and TCD detector to record online concentration data. The experimental test is performed in two steps:

1. Pre-reduction of the bi-functional compound at 900 °C in an N_2 flow with 10 vol% of H_2;
2. Steam reforming of methane and toluene. The operating conditions are provided in Table 2.

Table 2. Operating conditions of SERMT and SERM.

Operating Conditions	SERMT	SERM
Temperature (°C)	650	650
Pressure (atm)	1	1
CH_4 flow rate (Nml min^{-1})	75	75
N_2 flow rate (Nml min^{-1})	5.7	5.7
C_7H_8 flow rate (ml min^{-1})	4.33×10^{-3}	-
Water flow rate (ml min^{-1})	0.195	0.180
WHST (g_{cat} h Nl^{-1})	≈2	≈2
Ni-WHST (g_{cat} h Nl^{-1})	0.12	0.12

3. Results

3.1. Characterization

Characterization of sorbents and bi-functional materials was performed to evaluate their structural and textural properties by XRD, BET/BJH and SEM analyses and Ni species reducibility of bi-functional materials were also studied by TPR.

3.1.1. Characterization of Sorbents

XRD Analyses

XRD spectra of sorbents synthesized with 85 or 56 wt% of CaO are compared to C100 and May samples (Figure 2) and the sizes of the corresponding crystal of CaO and mayenite, evaluated by Scherrer formula, are reported in Table 3.

Finally, the mayenite sample (May) also presents the spinel phase ($CaAl_2O_4$) (Figure 2). The mayenite crystallite size is the lowest along our sorbents and is extremely similar to the C56 and C85 ones (Table 3).

Table 3. CaO and mayenite crystallites size in various sorbents.

Sample Name	Calcium Oxide Crystallites Size (nm)	Mayenite Crystallites Size (nm)
C100	32.0	/
C85	40.0	27.0
C56	36.5	26.6
May	/	25.6

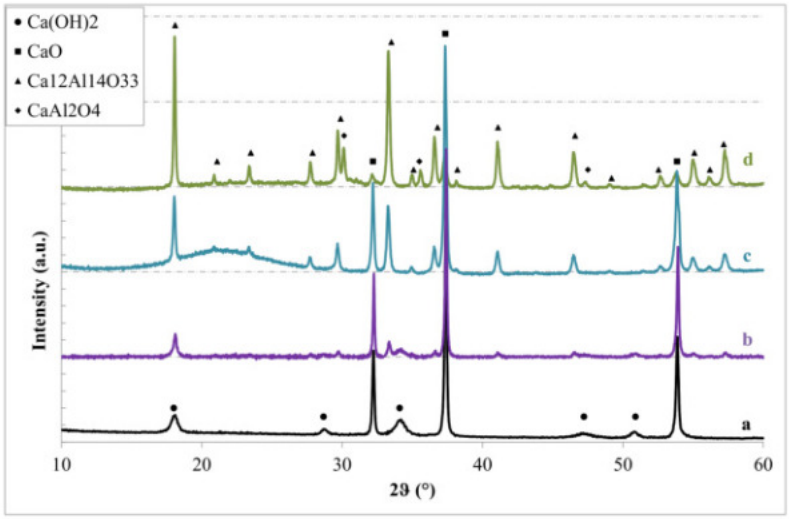

Figure 2. XRD of sorbents synthetized with various CaO contents (a) C100, (b) C85, (c) C56, and (d) May.

BET/BJH Analyses

Specific surface area, pore volume and average pore size values of various sorbents are contained in Table 4. Similar values are obtained for various structural properties in C100 and May samples. C56 presents the lowest value of the specific surface area and the highest value for average pore size. C85 has a slightly higher specific surface area and lower pore volume than C56.

Table 4. Specific surface area, pore volume and average pore size of various sorbents.

Sample Name	Specific Surface Area (m^2/g)	Pore Volume (cm^3/g)	Average Pore Size (nm)
C100	19.2	0.13	27.8
C85	12.2	0.05	15.9
C56	10.4	0.07	28.1
May	18.0	0.11	25.5

3.1.2. Characterization of Bi-Functional Materials

XRD: Crystallites Size and Precipitated Crystal Phase

The diffraction patterns of the bi-functional compounds obtained by impregnation (Figure 3) highlight the CaO sorbent phase at 2θ = 32.2°, 37.4°, 53.9°, 64.2° and 67.4°, the mayenite phase mainly at 2θ = 18.1°, 33.4°, 36.6°, 41.2° and 46.6°; and the bunsenite phase, cubic crystal form of NiO, for every bi-functional material at 2θ = 43.0°, its other rays being superposed to CaO and $Ca_{12}Al_{14}O_{33}$ phases.

The NiO crystallite size (Table 5) shows a maximum value for C100Ni3, whereas the CaO-mayenite supported sample (C56Ni3) has a crystallites dimension in the range of 23–24 nm; MayNi3 presents the lower NiO crystallite size.

Table 5. NiO and Ni (after TPR) crystallite size of bi-functional compounds.

Sample Name	NiO Crystallite Size (nm)	Ni Crystallite Size after Reduction (nm)
C100Ni3	33.8	n.a.
C56Ni3	23.8	37.8
MayNi3	17.9	n.a.

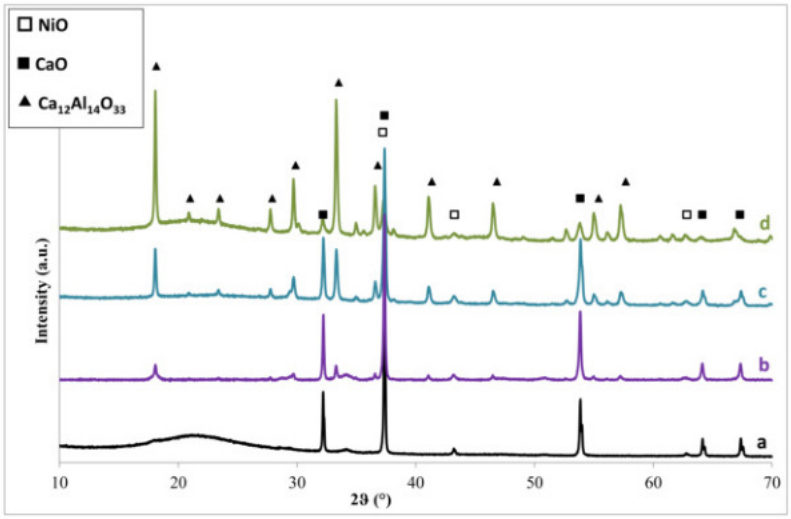

Figure 3. XRD patterns of (a) C100Ni3, (b) C85Ni3, (c) C56Ni3, and (d) MayNi3.

No substantial differences were observed for the samples impregnated with 6 wt% of Ni (spectra not shown).

BET/BJH Analyses: Impregnation Effect on Surface Area and Porosity

In Table 6, the specific surface area, pore volume and average pore size of the impregnated samples are reported.After the impregnation process, C100Ni3 shows (Table 6) specific surface area and pore volume decreases with a simultaneous increase in pore size (see Table 3). In general, for the other compounds, the impregnation process improves the surface characteristics; this synthesis step generates better textural properties.

Table 6. Specific surface area, pore volume and average pore size of bi-functional compounds.

Sample Name	Specific Surface Area (m^2/g)	Pore Volume (cm^3/g)	Average Pore Size (nm)
C100Ni3	7.8	0.02	39.2
C56Ni3	13.4	0.08	25.4
MayNi3	18.4	0.15	33.4
C56Ni6	7.9	0.06	21.7

The increase in the specific surface area for C56Ni3 is concomitant to the increase in pore volume, maintaining a constant pore size: more pores of the same size of the un-impregnated sorbent are formed. Compared to other CaO contents, C56Ni3 presents intermediate values of specific surface area and pore volume but the lowest value of pore size. The corresponding bi-functional material with 6 wt% of Ni shows the same low specific surface area as C100Ni3, but pore volume and pore size similar to C56Ni3.

TPR Temperature-Programmed Reduction: Ni Reducibility

The temperature-programmed reduction profile of the bi-functional compound containing 56 wt% of CaO is reported in Figure 4 (curve b). The curves of C100Ni3 (a) and MayNi3 (c) could be taken as a reference for the interaction between Ni and CaO and Ni and mayenite, respectively. In Table 7, the temperature of the maximum reduction peak, H_2 consumption and Ni reducibility percentage are reported.

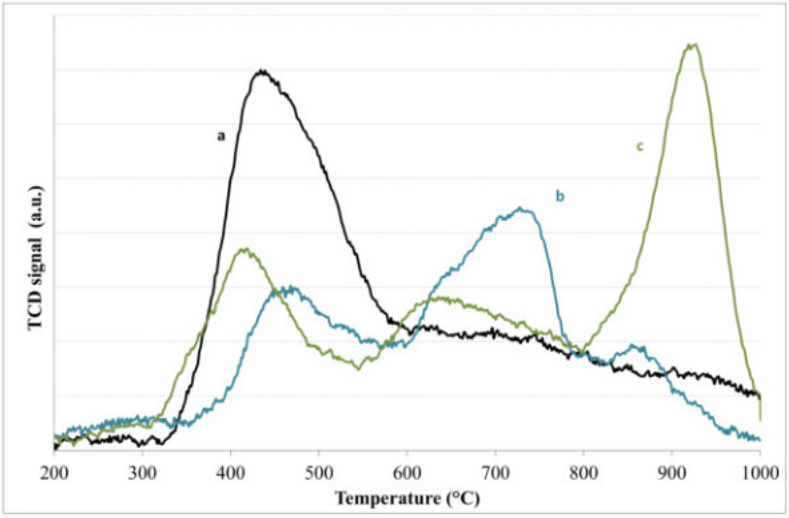

Figure 4. TPR profiles of (a) C100Ni3, (b) C56Ni3, and (c) MayNi3.

Table 7. Temperature of the maximum reduction peak, H_2 consumption and reducibility.

Sample Name	T_{max} (°C)	H_2 TPR (mmol/g)	Reducibility (wt%)
C100Ni3	436	0.474	2.78
C56Ni3	723	0.427	2.54
MayNi3	926	0.684	4.01

SEM

At low magnification (Figure 5a), the external particle morphology of C56Ni3 is displayed and exhibits homogeneous pore network and agglomeration. During the preparation of samples for the SEM analyses, sample C56Ni3 highlighted discrete mechanical resistance. C56Ni3 has an extremely regular morphology, and well-dispersed grains are also visible at higher magnification (Figure 5b).

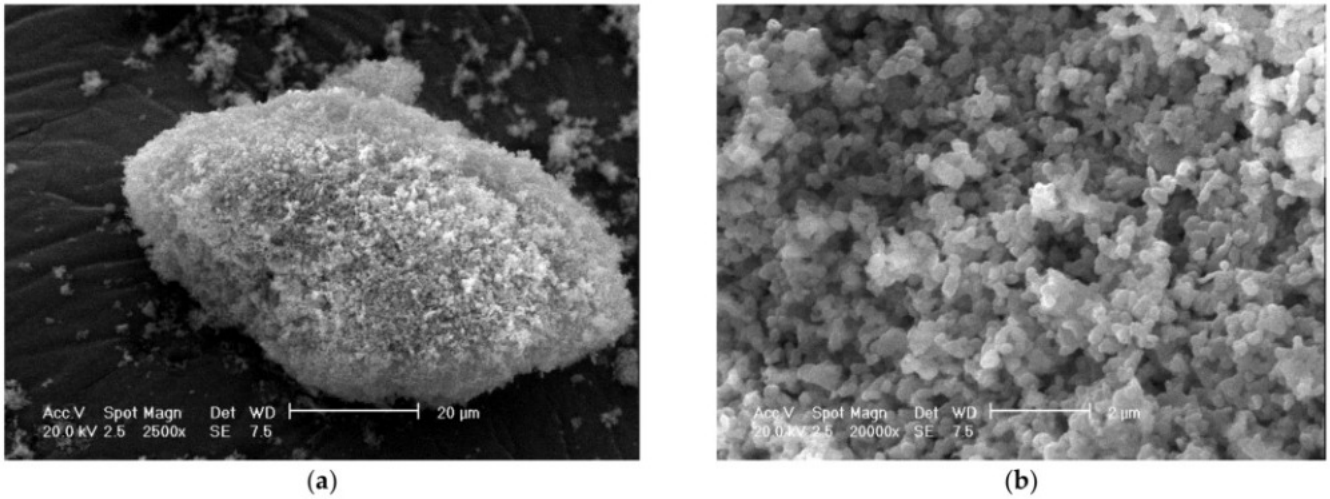

(**a**) (**b**)

Figure 5. SEM micrographies of C56Ni3 at differents magnifications (**a**) 2500×; (**b**) 20,000×.

3.2. Sorption Capacity (TGA)

In a first attempt to study CaO-mayenite sorbent systems, CO_2 sorption is performed on samples with different CaO amounts during 10 TGA cycles (Figure 6). A continuous decrease in CO_2 capture capacity (from 12.7 $molCO_2/kg_{sample}$ equals to 71.3% of the maxi-

mum thermodynamic sorption until 7.4 $molCO_2/kg_{sample}$ equal to 41.5% of the maximum thermodynamic sorption at the 10th cycle) can be ascribed to C100 (pure CaO sample, Figure 6a); a more stable behavior (although slightly decreasing) and a "self-activation" are detected for C85 (Figure 6b) and C56 (Figure 6c), respectively. No sorption capacity is attributable to the May sample (Figure 6d).

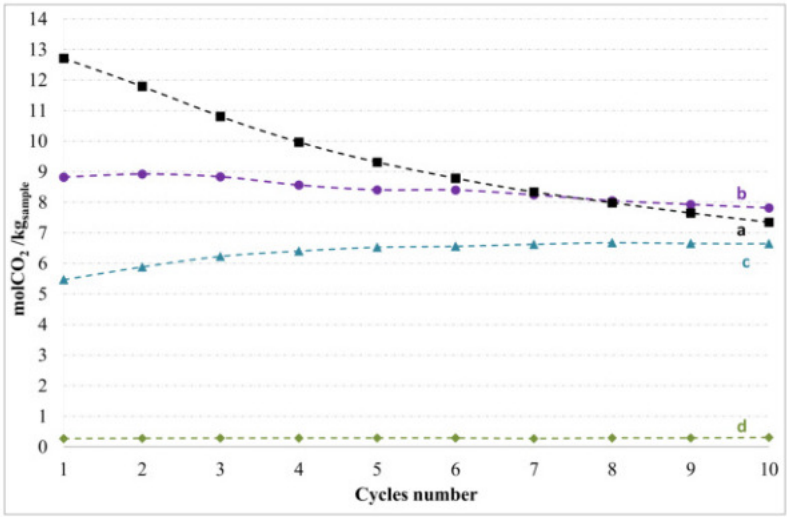

Figure 6. CO_2 sorption/desorption cycles TGA test of (a) C100 (b) C85, (c) C56, and (d) May.

The C56 sample has an initial CO_2 sorption value of 5.5 $molCO_2/kg_{sample}$ (56.7% of the thermodynamic sorption) and reaches an increased sorption capacity of 6.6 $molCO_2/kg_{sample}$ (68.0% of the thermodynamic sorption) at the 10th cycle (Figure 7).

The bi-functional compound C56Ni3 displays (Figure 7) an extremely fast carbonation regime, its carbonation increases smoothly with time and displays self-activation during cycles. At the 10th cycle, its CO_2 uptake increase up to 5.9 $molCO_2/kg_{sample}$ (60.8% of the thermodynamic sorption).

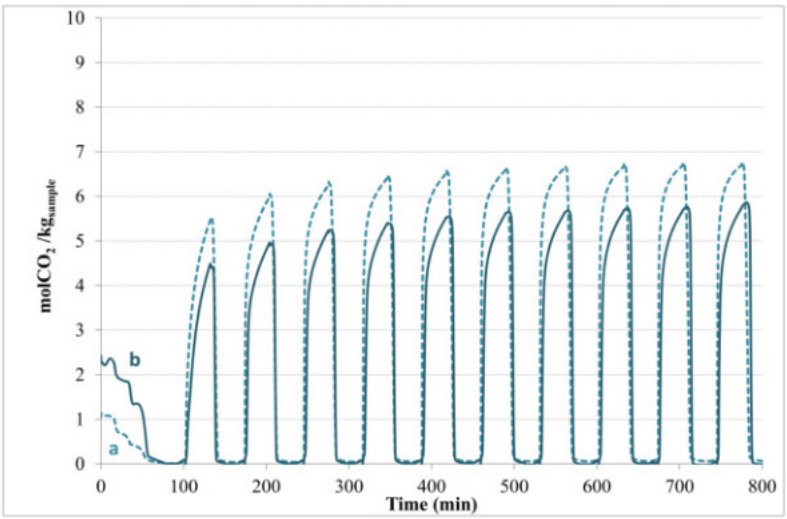

Figure 7. Cyclic CO_2 sorption/desorption TGA test: left: (a) C56, and (b) C56Ni3.

3.3. Reactivity of Bi-Functional Materials in a Fixed Bed Reactor

In steam reforming tests for toluene and methane, to work with a bi-functional material having both catalytic properties and CO_2 sorption capacity, the CaO-$Ca_{12}Al_{14}O_{33}$ sample has to be employed (C56Ni3); the unstabilized sorbent (C100Ni3) and catalyst (MayNi3) have also been evaluated in the same conditions for comparison.

3.3.1. Steam Toluene Reforming with Impregnated Samples

Steam toluene reforming reactivity for the 3 wt% Ni-impregnated samples is presented as H_2 and CO_2 molar flow rates (Figure 8) and explained as toluene conversion and benzene production as a by-product (Table 8). C100Ni3 sample shows a maximum H_2 production rate at the beginning of the test; afterwards, it slowly decreases. Until three hours of the test, it keeps almost a low activity in steam reforming and hydrogen production. CO_2 and benzene production show the same trend.

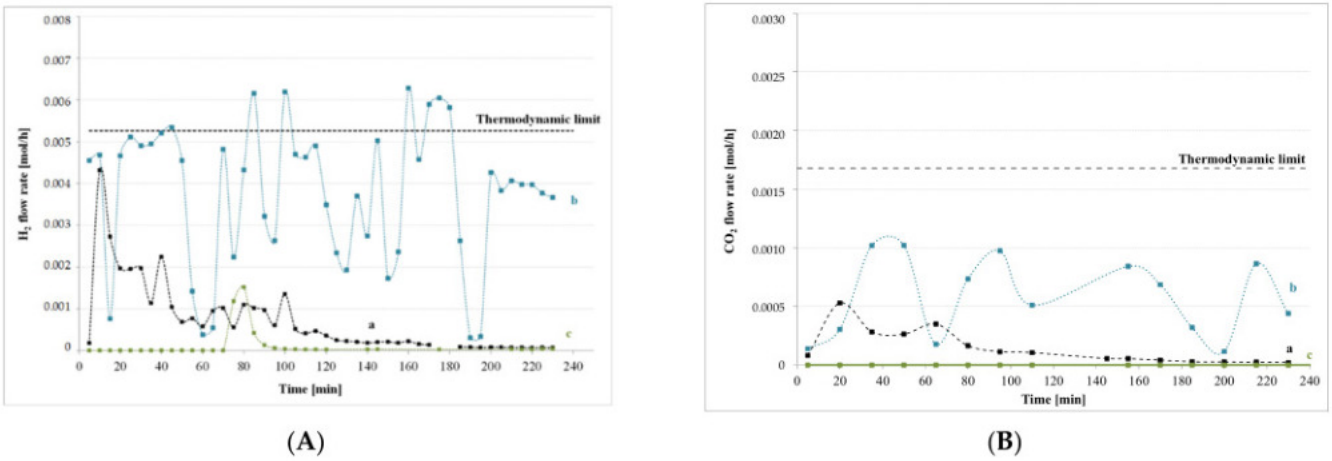

(**A**) (**B**)

Figure 8. Reactivity in steam toluene reforming tests at 640 °C for (a) C100Ni3, (b) C56Ni3, and (c) MayNi3. H_2 flow rate (**A**) and CO_2 molar flow (**B**).

In this set of tests, the C56Ni3 sample has a highly oscillatory trend: the toluene conversion (maximum 75%) is not complete. CO_2 is also produced with fluctuating values at a higher level than for C100Ni3 sample. On the contrary, benzene production is initially three times weaker than for C100Ni3 sample and remains at a stable mean value. Then, after 2 h of reaction, C100Ni3 and C56Ni3 samples present the same benzene production (Table 8).

Table 8. Toluene conversion of impregnated bi-functional compounds and corresponding benzene production as by-product.

Sample Name	Toluene Conversion at t = 15 min (%)	Toluene Conversion at t = 230 min (%)	Benzene Production at t = 15 min (µmol/h)	Benzene Production at t = 230 min (µmol/h)
C100Ni3	49	7	2.5	0.9
C56Ni3	20	75	0.4	1.0
MayNi3	0	0	0	0

MayNi3 sample shows no activity at the test beginning and small activity after 1 h of test and during 20 min; afterwards, it deactivates for the following 2 h of the test (Figure 9a). In order to better understand the behavior of the bi-functional compounds, steam methane reforming tests have been carried out on the C56Ni3 sample and the MayNi3 sample for comparison, with a compound possessing the only catalytic function.

3.3.2. Steam Methane Reforming with Impregnated Samples

Steam methane reforming reactivity for the 3 wt% Ni impregnated samples is presented as H_2 and CH_4 molar flow rates (Figure 9) and also expressed in terms of methane conversion.

The first results obtained with the C56Ni3 sample (Figure 9) indicate a deactivation from the first 40 min of the test. During this period, H_2 yield is lower (from 59% vol to less than 10% vol) than the thermodynamic value (75.5 vol%) and CH_4 conversion decreases

from 75% to less than 10%, not allowing to observe the enhancement due to CO_2 capture nor a stable methane reforming.

The same reactivity test with MayNi3 sample shows H_2 production close to the thermodynamic value and almost total CH_4 conversion (Figure 9).

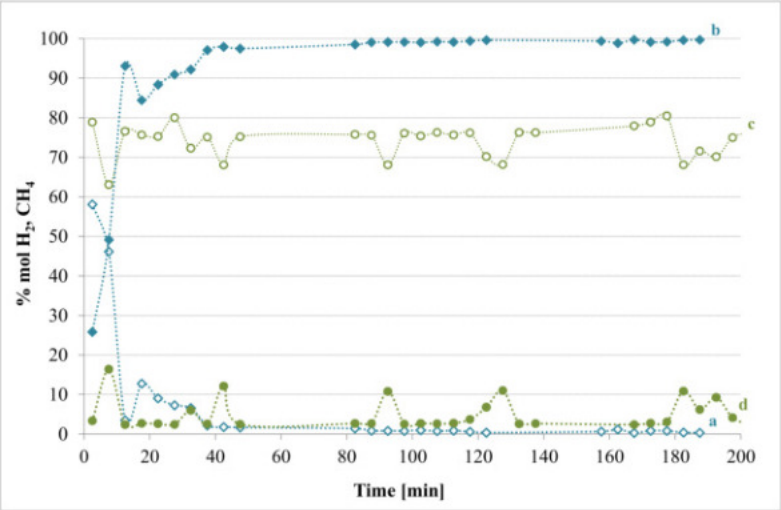

Figure 9. (a) H_2 and (b) CH_4 mol% during the SEMR with C56Ni3 and (c) H_2 and (d) CH_4 mol% during the SEMR with MayNi3.

In the next section, sorption enhanced steam reforming of methane and toluene are studied on higher Ni content bi-functional compounds (6 wt% of Ni) with various CaO contents. Tar syngas feeding and particle size diameter were compatible with fluidized pilot/industrial scale (355 μm < d_p < 1000 μm) [35], in order to stress more the bi-functional system and better understand its catalytic and sorption characteristics.

3.4. Reactivity of Bi-Functional Materials in a Fixed Bed Reactor with Higher WHST

A pre-reduction step of the bi-functional impregnated materials (C100Ni6, C56Ni6, and MayNi6) is conducted at 900 °C with a stream of 10 vol% of H_2 in N_2. The bi-functional compound (C85Ni6) has not been tested because the TGA analysis demonstrated a slight decrease in its CO_2 sorption capacity.

Steam reforming tests were performed at 650 °C, by simultaneously feeding toluene (0.0043 Nml min^{-1}), methane (75 Nml min^{-1}) and water (0.195 ml min^{-1}) with 9 g of sample, leading to a higher WHST value (Table 2).

The C100Ni6 sample displays a maximum H_2 production of 78.0 vol% (Figure 10a). In this case, the enhanced reforming of methane and toluene, and relative CO_2 capture, is blocked after 10 min, but the SERT remains stable during the whole test.

The bi-functional compound (C56Ni6) exhibits the best behavior (Figure 10b), reaching a maximum of H_2 production of 91.6 vol%. A sudden deactivation of the material follows, then the methane backs to the initial value and hydrogen sharply decreases before the complete deactivation around 10 min.

Furthermore, a SERMT test was carried out on the impregnated mayenite (MayNi6), in order to investigate its catalytic potential and the reason for its deactivation in methane reforming. Results (Figure 10c) indicate a good and stable performance (74.3 vol% H_2), confirmed by the extremely close value to thermodynamic limit (75.5 vol% H_2) and higher value than Ni commercial catalyst (72.5 vol% H_2), similarly to the performance of MayNi3.

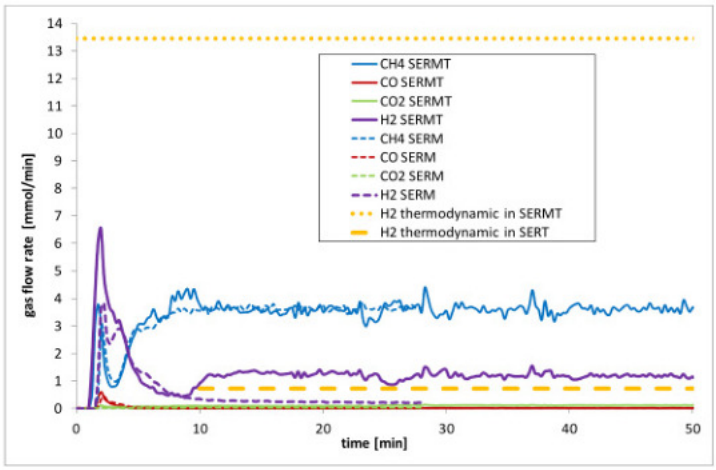

(**a**)

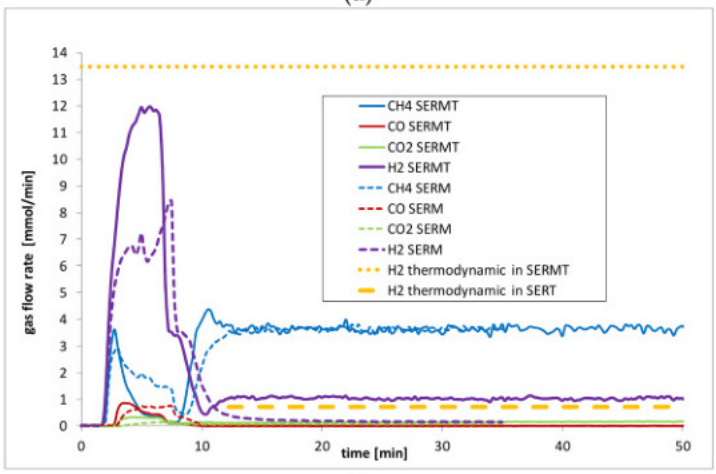

(**b**)

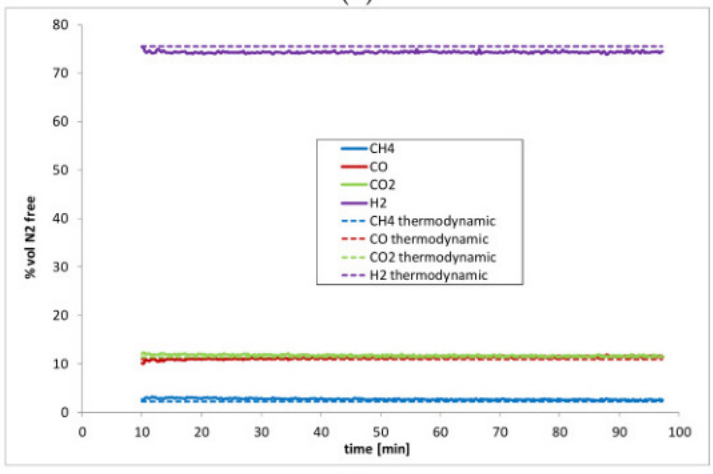

(**c**)

Figure 10. Sorption Enhanced Reforming of Methane (SERM) and Sorption Enhanced Reforming of Methane and Toluene (SERMT) tests on (**a**) C100Ni6, and (**b**) C56Ni6, (**c**) MayNi6.

In Table 9, the most relevant parameters and results achieved are summarised.

All the tested materials show almost complete conversion of toluene. Catalysts (MayNi6 and Ni commercial) are also efficient in steam methane reforming, with a slightly higher conversion for the first one. These results are confirmed by the best H_2 production reached on the bi-functional material C56Ni6. The worst performance can be attributed to C100Ni6 (without mayenite) with the lower methane conversion.

Table 9. Impregnated samples summary results.

Sample Name	Pre-breakthrough Time (min)	Toluene Conversion (%)	Methane Conversion (%)	H_2 (vol%)	WHST (g_{cat} h Nl^{-1})	Ni-WHST (g_{cat} h Nl^{-1})
C100Ni6	5	99.9	73.1	78.1	1.97	0.12
C56Ni6	10	99.9	88.2	91.6	1.60	0.10
MayNi6	-	99.9	87.9	74.3	1.32	0.08
Ni commercial catalyst	-	99.9	86.2	72.5	1.87	0.11

3.5. After Test Characterization

3.5.1. XRD

The following XRD analyses do not show any carbonate phase formation (Figure 11). Calcium carbonate is not present in any diffraction patterns of samples after test except for C100Ni3 sample, and the sorbent phase is still visible.

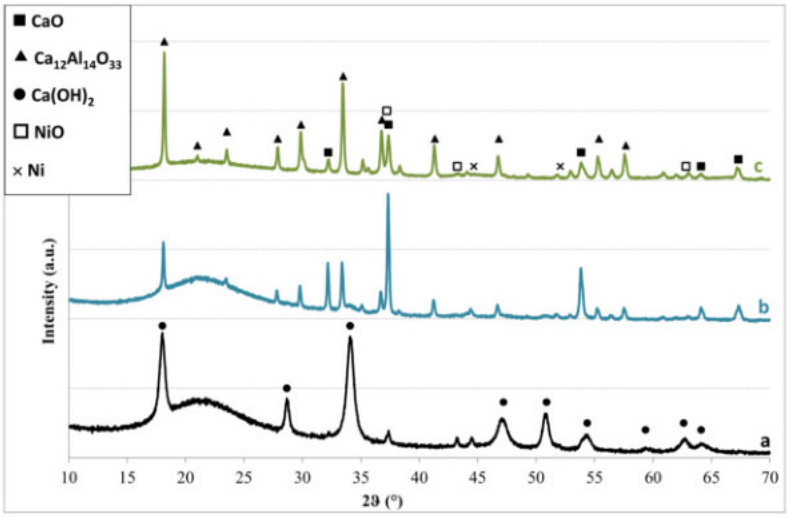

Figure 11. XRD analysis of bi-functional compounds after toluene reforming test: (a) C100Ni3, (b) C56Ni3, and (c) MayNi3.

In the C56Ni3 sample, nickel species are totally reduced in Ni^0. In the C100Ni3 sample, both NiO and Ni^0 are visible and this sample is hydroxylated to portlandite, a highly visible phase in its diffracted pattern at $2\theta = 18.1°, 34.2°, 50.9°$ (main rays), also visible in C100Ni6.

The crystallite size of NiO in C100Ni3 and MayNi3 does not increase during toluene reforming (33.4 nm and 18.4 nm, respectively) and decreases with mayenite content increase, as before the test (Table 5). The Ni^0 crystallite size after toluene reforming is similar for C100Ni3 (28.3 nm) and C56Ni3 (25.5 nm) and lower than in the corresponding sample after TPR (Table 5).

3.5.2. BET/BJH

The impregnated mayenite (MayNi3) characterized after the test (Table 10) does not show significant differences compared to the values of BET and BJH analysis before the test (Table 10). For C100Ni3 and C56Ni3 samples, pore volume and average pore size decrease dramatically (about 30% to 50% and about 50%, respectively). The 6 wt% Ni impregnated sample (C56Ni6) shows a strong decrease in all the parameters: about 50% for specific surface area and pore volume and about 30% in average pore diameter.

Table 10. Specific surface area, pore volume and average pore size of bi-functional compounds after test.

Sample Name	Specific Surface Area (m^2/g)	Pore Volume (cm^3/g)	Average Pore Size (nm)
C100Ni3 after test	9.3	0.04	17.9
C56Ni3 after test	12.4	0.06	12.8
MayNi3 after test	18.5	0.15	32.6
C56Ni6 after test	4.1	0.02	14.4

3.5.3. SEM-EDX

All impregnated samples containing 6 wt% of Ni show carbon deposition in optical microscopic pictures (see [33]), and in SEM-EDX analysis, the carbon is highlighted close to the highest Ni concentration as an example for C56Ni6 sample.

4. Discussion

4.1. Characterization of Sorbents

4.1.1. XRD Analyses

In the characterization of sorbents, the XRD spectrum of the C100 indicates extremely well-defined CaO rays at 2θ = 32.1°, 37.3°, and 53.8° (Figure 2a). The presence of calcium hydroxide in this sample is due to the ambient humidity recovered by the sample during its storage. This sample presents calcium oxide crystallites at the size of 32 nm (Table 3), a value already found by Zamboni et al. [13].

The wet mixing synthesis method has allowed the formation of mayenite on CaO (Figure 2b,c) with different intensities depending on mayenite content, and similar crystallite sizes of mayenite and calcium oxide for C85 and C56 (Table 3).

The mayenite sample (May) also presents the spinel phase ($CaAl_2O_4$) (Figure 2d), already found from $CaCO_3$ and Al_2O_3 precursors mixed in a planetary ball mill and annealed at 900 °C [36]. From the binary diagram of CaO and Al_2O_3, a temperature higher than 1300 °C with the proper molar ratio of CaO/Al_2O_3 = 12/7 is needed to allow the solid-state synthesis of mayenite [37]. In May compound, mayenite crystallite size is the lowest along our sorbents but is extremely similar to C85 and C56 ones (Table 3).

All the expected crystalline phases are evident in these spectra.

4.1.2. BET/BJH Analyses

If the results of BET and BJH methods (Table 4) indicate intermediate values of specific surface area and pore volume for C85 and C56 samples compared to C100 and May samples, it is important to note that the higher average pore size is obtained for C56 sample and the lower one for C85.

For corresponding impregnated bi-functional compounds, in Figure 3, neither mixed calcium-nickel nor aluminium-nickel phase are visible after the impregnation with $Ni(NO_3)_2$ $6H_2O$. The absence of such a mixed phase is important both for the CO_2 sorption stability and for the catalytic activity. In fact, the availability of both CaO, and Ni phases is necessary to ensure the CO_2 sorption by CaO, and the catalytic effect by reducible Ni phases.

The decrease of the NiO crystallite size with the mayenite content increase confirms the dispersant mayenite role (Table 5). The Ni^0 crystallite size is observed at a higher value (38 nm) when the sample is reduced until 1000 °C, under a He/H_2 mixture containing 10% of H_2 because of the severe conditions used.

C100Ni3 shows (Table 6) specific surface area and pore volume decreases with a simultaneous increase in pore size (see Table 3), probably due to the coalescence phenomenon during which smaller pores grow together to form bigger ones, that decreases the specific surface area and total pore volume. The low CaO-Ni interaction could explain the decrease in textural characteristics. In general, for the other compounds, the impregnation process improved the surface characteristics; this synthesis step generated better textural properties. From a certain point of view, the impregnation process could work as the hydration process

often used to increase the morphological characteristics of the solid sorbents [24]. In fact, most probably during the first step of this process, CaO dispersed on the mayenite reacts with water to form $Ca(OH)_2$ and, at the same time, the metal salt starts to diffuse into the solid. When the final product is thermally treated, a double effect is summed: the dehydration of $Ca(OH)_2$ and the thermal decomposition of the metal nitrate.

The low concentration of the metallic salt avoids the problem of the pore mouths blocking, hence a reduction of the porosity.

4.1.3. TPR Analyses

In the TPR curves (Figure 4), the Ni-CaO interaction produces a slight increase in the reduction temperature (436 °C) that is slightly higher than the reduction temperature presented by NiO itself (420 °C) but is still weak. The intermediate peaks between 550 °C and 750 °C could be attributed to the Ni-$Ca_{12}Al_{14}O_{33}$ interaction also reported by Cesario et al. [19]. At the highest temperature (>800 °C), a small reduction peak is visible for the sample containing 56 wt% of CaO (curve b), whereas, for MayNi3 (curve c), this is the main one. This high temperature of H_2 consumption can be associated with the mayenite oxygen mobility [38] and to a lesser extend (not observed by XRD) to the reduction of Ni oxide in a spinel phase ($NiAl_2O_4$) which needs a high temperature (>800 °C) in order to be reduced [39]. In Table 7, the higher the mayenite content, the higher the reduction temperature, and the higher H_2 consumption is due to the increase in oxygen mobility in the mayenite structure with a high temperature. In fact, mayenite did not reduce (not a change of structure), but it can release oxygen and then limit the Ni species reduction. This phenomenon also explains the reducibility value higher than the theoretical Ni content (3 wt%) for the MayNi3 sample.

This analysis highlighted the interaction between Ni-sorbent, Ni-support and specific mayenite behavior associated with its oxygen mobility.

4.1.4. TGA Testes

Before the reactivity performance for sorption enhanced reactions, the sorption capacity of synthesized material was investigated in cyclic TGA tests (Figures 6 and 7). C100 is fast deactivated (Figure 6a), confirming the well know phenomenon of sintering [2]: at the first cycle, it absorbs 12.7 $molCO_2/kg_{sample}$ equal to 71.3% of the maximum thermodynamic sorption and its sorption capacity decreases until 7.4 $molCO_2/kg_{sample}$ (41.5% of the maximum thermodynamic sorption) at the 10th cycle. After seven cycles, it shows a lower capacity than C85 (Figure 6b) and continues to decrease. This tendency is in agreement with various studies [2,3,21]. On the other side, the May compound shows an extremely small sorption capacity (Figure 7), due to residual CaO in the structure (see XRD section). The most interesting behavior is the "self-activation" detected for C85 (Figure 6b), reaching the stable value after five cycles.

Both C56 and C85 sorbents display an initial activation time, already found and defined [24] as a self-activation due to a slower regime in which the reaction rate is likely limited by both the diffusion of CO_2 through the initial $CaCO_3$ layer formed during the carbonation reaction [40] and the presence of $Ca_{12}Al_{14}O_{33}$ intimate surrounding CaO grains [21]. C85 has a deactivation trend during the 10 cycles, which is confirmed during the 20 following cycles (not shown), and after 29 cycles, reaches the sorption uptake performed by C56 (6.3 $molCO_2/kg_{sample}$); the latter has a quite stable behavior after the 8th cycle (62.0% of the maximum thermodynamic sorption). The deactivation of the C85 sorbent is likely due to the smaller amount of $Ca_{12}Al_{14}O_{33}$ than in the C56 sorbent, but also to its lower pore size and pore volume. Therefore, in order to assure a good cyclic stability operation (strictly required for industrial application), hereafter the development of CaO/ $Ca_{12}Al_{14}O_{33}$ system is carried on samples with a CaO amount of 56 wt%.

CO_2 breakthrough profile of the C56 sorbent (Figure 7 (a)) is characterized by a fast carbonation reaction (kinetic regime) occurring during the first seconds of the whole process, then the carbonation rate gently decreases for the duration of the carbonation test

and the formation of a $CaCO_3$ shell. These exhibit values are in agreement with ones in literature [32]. The enhancement in CO_2 uptake of this bi-functional compound can be explained by the high increase in specific surface area (73%) and in pore volume (25%), and the rearrangement of pore distribution size (smaller pores are formed).

Although textural characteristics of the C56Ni3 sample improve as well after the impregnation process, with specific surface area increases of 29% and pore volume of 25%, pore distribution size does not change (Tables 3 and 6); moreover, the presence of the metal phase generates different interaction between Ni and $Ca/Ca_{12}Al_{14}O_{33}$. Some authors who studied this ternary system already observed an increase in surface area [19] and in sorption capacity, but the thermal treatment temperature used after the impregnation process was much lower (750 °C), or a double thermal treatment with the final one up to 900 °C for 1 h was used [41]. Finally, the impregnation process does not modify drastically the sorption capacity of the C56 sorbent.

After 10 calcination/carbonation TGA cycles (Figures 6 and 7), the C56 sorbent and C56Ni3 catalyst present three main phases observed by XRD. Mayenite ($Ca_{12}Al_{14}O_{33}$) diffraction rays are observed, and both CaO and $CaCO_3$ (calcite crystalline phase) are diffracted in every sample, pointing out that the carbonation reaction occurred but not completely, as the TGA analyses highlighted, and that after the last cycle during the cooling down of the system, the sorbent was partially regenerated. The CaO crystallite sizes of these samples after 10 TGA cycles are 34.2 nm and 32.7 nm for C56 and C56Ni3, respectively. These values are extremely close, even smaller than in the fresh corresponding samples (36.5 nm and 36.6 nm, respectively), indicating that no CaO sintering appears after 10 cycles for these samples containing 44 wt% of mayenite. The sorption function of this material is efficient and stable with carbonation/regeneration cycles, and can be tested in steam toluene reforming.

4.2. Reactivity Tests

4.2.1. Steam Toluene Reforming Tests

During steam toluene reforming tests (Section 3.3.1), the C100Ni3 sample, showing Ni crystallites in weak interaction with CaO, is quickly deactivated (Figure 8a). The low interaction between CaO and Ni has been reported by several authors and leads to rapid carbon formation at the surface. The C100Ni3 sample shows activity towards benzene production thanks to thermal cracking or steam dealkylation.

C56Ni3 presents a more stable behavior that can be explained by several characteristics. The lower NiO particle size of this sample (Table 5) favors the reactivity and probably limits carbon formation. The different TPR shapes, hence the different Ni species in interaction with the support, influence the reforming behavior. Here, Ni crystallites in weak interaction with CaO (as in C100Ni3 sample) are associated with Ni crystallites in stronger interaction with CaO, reducible between 600–800 °C (Figure 4). At the steam reforming temperature (640 °C), part of these Ni species is reduced and then active, but their sintering is limited by their interaction with CaO and mayenite. A possible reason for CO_2 oscillating behavior could be the oxidation of carbon formed on the Ni active sites by the "free oxygen" of mayenite or a progressive activation of the Ni species by the reducing atmosphere (in situ).

The null activity of the MayNi3 sample could be associated with the low quantity of reducible nickel species observed by TPR (Figure 8) at the reforming temperature. In fact, the larger part of Ni species reduction takes place above 800 °C.

During steam methane reforming tests (Section 3.3.2) performed after reduction of the sample, the fast deactivation of this C56Ni3 compound (Figure 9), implies that it would not be able to operate reforming under typical syngas composition, but the high conversion and stability of the MayNi3 catalyst confirms the important role of mayenite in the steam methane reforming thanks to the improvement of Ni species dispersion.

4.2.2. Sorption Enhanced Steam Reforming of Methane and Toluene

The results from sorption-enhanced steam methane reforming literature suggest increasing Ni percentage in order to have higher conversion and stability [42]. Cesario et al. [18] reached 100 mol% of H_2 production using a Ni-CaO-mayenite bi-functional compound with 5 wt% of Ni and 75% of CaO. Radfarnia et al. [43] found a methane conversion of 99.1% using a supported sorbent/catalyst system based on Ni-CaO-$Ca_9Al_6O_{18}$ with 25 wt% of Ni. Kim et al. [44] studied the Ni-CaO-mayenite system with different Ni amounts (from 3 to 10 wt%) with a fixed CaO content of 75 wt% and found the optimum (95 vol% of H_2 production and 100% of CH_4 conversion) when the Ni amount is fixed at 7 wt%.

The reduction curves of bi-functional impregnated materials with 6 wt% of Ni, (not reported) shown Ni-CaO and Ni-mayenite interactions. The Ni-CaO interactions produce an increase in the reduction temperature (420 °C), and the intermediate peaks between 550 °C and 750 °C can be attributed to the Ni-$Ca_{12}Al_{14}O_{33}$ interaction. The estimated percentages of nickel from the pre-reduction curves of bi-functional materials indicate that the lower content of CaO in the sample is associated with the lower available Ni^0 from pre-reduction. In fact, the higher mayenite content is associated with the higher reduction temperature (see TPR Temperature-Programmed Reduction: Ni Reducibility) as observed for the bi-functional compounds containing 3 wt% of Ni.

In any case, all bi-functional compounds showed a fast deactivation for the methane reforming (Figure 10), probably due to the calcium carbonate formation or carbon deposition over the particles. Just after the deactivation of C56Ni6 occurred in the first 10 min of the test (Figure 10b), an average flow of hydrogen was produced (1.045 mmol min^{-1}), slightly higher than the thermodynamic value calculated at the same toluene test conditions (0.723 mmol min^{-1}), with a CO_2 flow (0.161 mmol min^{-1}), less than its thermodynamic limit (0.275 mmol min^{-1}). This could be explained by the residual capture of CO_2 from the sorbent or steam gasification of carbonaceous deposits [45].

On the other hand, catalysts (MayNi6 and Ni commercial, in Table 9) are efficient in methane and toluene steam reforming, with a slightly higher conversion for the first one, by confirming improvement of performance due to the mayenite support. These results are confirmed by other authors [46], and by the best H_2 production (Table 9) reached on the bi-functional material C56Ni6 (> 91 vol%). This result is highly encouraging compared to recent studies. Pecharaumpon et al. [47] reported similar results (93 vol% H_2) with higher nickel content (12.5 wt%) in their bi-functional material and Nimmas et al. [48] indicate slightly lower results (87 vol% of H_2) with similar nickel content (4.7 wt%) in their developed material, respectively. The worst performance can be attributed to C100Ni6 (without mayenite).

On all combined samples, the SERMT never overcomes the first 10 min, and sole toluene reforming, close to the thermodynamic value, remains active after this pre-breakthrough period. The fast deactivation could be due to a clogging effect of the calcium carbonate that reduces Ni accessibility, or to some carbon deposition on the catalyst, no longer able to reform a stable molecule as methane.

The C56Ni6 sample gives a hydrogen production of.0.368 mmol min^{-1} g^{-1}.

4.3. Post-Tests Characterization

In the post-tests XRD analyses post, the sorbent phase is still visible; this behavior could be explained by the remarkably low CO_2 partial pressure that, at 640 °C, determines a point under the thermodynamic CaO carbonation/calcination curve, lying in the calcination area. In every sample with 6 wt% of Ni^0, the calcium carbonate phase is detected confirming CO_2 sorption activity (not shown). Only the metallic Ni^0 phase is detected, NiO phase is completely reduced after the pre-reduction step and not re-oxidized during the reaction. In addition to the mayenite phase present in every bi-functional compound, the formation of a metastable phase $Ca(AlO_2)_2$ is found, probably related to the presence of $CaCO_3$ and Al_2O_3 at high temperature [49]. The stability of Ni particle size, particularly in the C56Ni3

(25.5 nm) sample is extremely important to avoid catalyst deactivation and is associated with the mayenite phase presence.

By comparing pre-tests BET/BJH results (Table 6), C56Ni3 and C56Ni6 pore volume and pore size strongly decrease, probably because of pore mouths blocking due to calcium carbonate formation and carbon deposition.

The results of SEM-EDS point out the carbon formation from the Boudouard reaction taking place on the supported catalyst during the sorption enhanced reactions and causing the catalyst deactivation on bi-functional sorbent/catalyst compounds. Deposited carbon (0.57 wt%) was detected by TGA also on C56Ni3 sample, probably causing the spaced-out deactivation of the sample during SERT.

5. Conclusions

The bi-functional compounds composed by 3 wt% of metallic Ni, an extremely low value, selected in order to decrease the environmental safety problems connected to Ni toxicity, are not particularly active; in particular, the C56Ni3 sample showed fluctuating activity in SERT.

The impregnated sorbents did not show any Ca-Ni mixed phases by XRD; their reducibility, on average, was evaluated equal to 80%. From the TPR curves, in any case, different Ni-morphologies or interactions with the support are detected and could explain the different catalytic behaviors. The MayNi3 sample did not show activity because of the impossibility of being reduced in situ under the chosen conditions.

The results with 3 wt% of Ni show that the hydrogen enhancement has not been observed because of the extremely small amount of CO_2 produced during the reaction, not enough to allow the carbonation reaction. For this reason, additional tests of sorption enhanced reforming of methane and toluene have been performed at higher Ni-WHST (about 0.12 g_{cat} h Nl^{-1}) and with a higher Ni amount. Every 6 wt% of Ni impregnated samples can reform toluene with 99.9% of conversion, but the simultaneous reforming of methane usually falls down after 10–15 min. SERT is well visible; in actuality, the hydrogen amount produced by the only toluene reaction is higher than the thermodynamic equilibrium value, indicating an efficient simultaneous CO_2 sorption.

On the other hand, from the point of view of the methane reforming, it can be concluded that the intimate mixing between the sorbent and catalyst is not favorable, and further studies could tend to employ a mechanical mixing of the two materials (sorbent and catalyst) rather than the synthesis of a bi-functional single particle.

Most likely, the rapid deactivation of the material can be linked to the formation of carbon deposits because the Ni-CaO interactions make the nickel present for the reforming of methane inaccessible, or the volume increase related to the carbonated CaO may decrease the accessibility to the catalytic phase from reactants.

Author Contributions: The following statements should be used Conceptualization, F.M., C.C., K.G.; methodology, F.M., C.C., K.G.; investigation, F.M., E.M., C.C., K.G.; resources, C.C., K.G.; data curation, F.M., E.M.; writing—original draft preparation, F.M., E.M.; writing—review and editing, C.C., K.G.; visualization, F.M., E.M., C.C., K.G.; supervision, C.C., K.G.; project administration, C.C., K.G.; funding acquisition, C.C., K.G. All authors have read and agreed to the published version of the manuscript.

Funding: The financial support of European Contract 299732 UNIfHY is kindly acknowledged (UNIQUE for HYdrogen production, funded by FCH-JU under the topic SP1-JTI-FCH.2011.2.3: Biomass-to-Hydrogen thermal conversion processes).

Institutional Review Board Statement: Not applicable.

Informed Consent Statement: Not applicable.

Data Availability Statement: Francesca MICHELI, PhD Thesis, University of L'Aquila, April 2015.

Conflicts of Interest: The authors declare no conflict of interest. The funders had no role in the design of the study; in the collection, analyses, or interpretation of data; in the writing of the manuscript, or in the decision to publish the results.

References

1. Rufford, T.E.; Chan, K.I.; Huang, S.H.; May, E.F. A review of conventional and emerging process technologies for the recovery of helium from natural gas. *Adsorpt. Sci. Technol.* **2014**, *32*, 49–72. [CrossRef]
2. Grasa, G.S.; Abanades, J.C. CO_2 capture capacity of CaO in long series of carbonation/calcination cycles. *Ind. Eng. Chem. Res.* **2006**, *45*, 8846–8851. [CrossRef]
3. Abanades, J.C. The maximum capture efficiency of CO_2 using a carbonation/calcination cycle of $CaO/CaCO_3$. *Chem. Eng. J.* **2002**, *90*, 303–306. [CrossRef]
4. Borgwardt, R.H.; Roache, N.F.; Bruce, K.R. Method for variation of grain size in studies of gas-solid reactions involving CaO. *Ind. Eng. Chem. Fundam.* **1986**, *25*, 165–169. [CrossRef]
5. Florin, N.H.; Harris, A.T. Enhanced hydrogen production from biomass with in situ carbon dioxide capture using calcium oxide sorbents. *Chem. Eng. Sci.* **2008**, *63*, 287–316. [CrossRef]
6. Mattisson, T.; Garcıa-Labiano, F.; Kronberger, B.; Lyngfelt, A.; Adanez, J.; Hofbauer, H. Chemical-looping combustion using syngas as fuel. *Int. J. Greenhouse Gas Control* **2007**, *1*, 158–169. [CrossRef]
7. Qiao, C.; Xiao, Y.; Xu, X.; Zhao, L.; Tian, W. Comparative analysis of hydrogen production systems from biomass based on different absorbent regeneration processes. *Int. J. Hydrogen Energy* **2007**, *32*, 80–85. [CrossRef]
8. Di Felice, L.; Courson, C.; Jand, N.; Gallucci, K.; Foscolo, P.U.; Kiennemann, A. Catalytic biomass gasification: Simultaneous, hydrocarbons steam reforming and CO_2 capture in a fluidised bed reactor. *Chem. Eng. J.* **2009**, *154*, 375–383. [CrossRef]
9. Corella, J.; Toledo, J.M.; Molina, G. Steam gasification of coal at low-medium (600–800 °C) temperature with simultaneous CO_2 capture in fluidized bed at atmospheric pressure: The effect of inorganic species. 1. Literature review and comments. *Ind. Eng. Chem. Res.* **2006**, *45*, 6137–6146. [CrossRef]
10. Koppatz, S.; Pfeifer, C.; Rauch, R.; Hofbauer, H.; Marquard-Moellenstedt, T.; Specht, M. H_2 rich product gas by steam gasification of biomass with in situ CO_2 absorption in a dual fluidized bed system of 8 MW fuel input. *Fuel Process. Technol.* **2009**, *90*, 914–921. [CrossRef]
11. Zamboni, I.; Courson, C.; Kiennemann, A. Synthesis of Fe/CaO active sorbent for CO_2 absorption and tars removal in biomass gasification. *Catal. Today* **2011**, *176*, 197–201. [CrossRef]
12. D'Orazio, A.; Di Carlo, A.; Dionisi, N.; Dell'Era, A.; Orecchini, F. Toluene steam reforming properties of CaO based synthetic sorbents for biomass gasification process. *Int. J. Hydrogen Energy* **2013**, *38*, 13282–13292. [CrossRef]
13. Zamboni, I.; Courson, C.; Niznansky, D.; Kiennemann, A. Simultaneous catalytic H_2 production and CO_2 capture in steam reforming of toluene as tar model compound from biomass gasification. *Appl. Catal. B.* **2014**, *145*, 63–72. [CrossRef]
14. Han, S.J.; Song, J.H.; Yoo, J.; Park, S.; Kang, K.H.; Son, I.K. Sorption-enhanced hydrogen production by steam reforming of ethanol over mesoporous $Co/CaO\text{-}Al_2O_3$ xerogel catalysts: Effect of Ca/Al molar ratio. *Int. J. Hydrogen Energy* **2017**, *42*, 5886–5898. [CrossRef]
15. Li, Z.S.; Cai, N.S.; Huang, Y.Y.; Han, H.J. Synthesis, experimental studies, and analysis of a new calcium-based carbon dioxide absorbent. *Energy Fuels* **2005**, *19*, 1447–1452. [CrossRef]
16. Feng, B.; Liu, W.; Li, X.; An, H. Overcoming the problem of loss-in-capacity of calcium oxide in CO_2 capture. *Energy Fuels* **2006**, *20*, 2417–2420. [CrossRef]
17. Li, Z.S.; Cai, N.S.; Huang, Y.-Y. Effect of preparation temperature on cyclic CO_2 capture and multiple arbonation-calcination cycles for a new Ca-based CO_2 sorbent. *Ind. Eng. Chem. Res.* **2006**, *45*, 1911–1917. [CrossRef]
18. Cesario, M.R.; Barros, B.S.; Zimmermann, Y.; Courson, C.; Melo, D.M.A.; Kiennemann, A. CO_2 sorption enhanced steam reforming of methane using $Ni/CaO{\cdot}Ca_{12}Al_{14}O_{33}$ catalysts. *Adv. Chem. Lett.* **2013**, *1*, 292–299. [CrossRef]
19. Cesario, M.R.; Barros, B.S.; Courson, C.; Melo, D.M.A.; Kiennemann, A. Catalytic performances of Ni–CaO–mayenite in CO_2 sorption enhanced steam methane reforming. *Fuel Process. Technol.* **2015**, *131*, 247–253. [CrossRef]
20. Zamboni, I.; Zimmermann, Y.; Kiennemann, A.; Courson, C. Improvement of steam reforming of toluene by CO_2 capture using $Fe/CaO\text{-}Ca_{12}Al_{14}O_{33}$ bi-functional materials. *Int. J. Hydrogen Energy* **2015**, *40*, 5297–5304. [CrossRef]
21. Martavaltzi, C.S.; Lemonidou, A.A. Parametric study of the $CaO\text{-}Ca_{12}Al_{14}O_{33}$ synthesis with respect to high CO_2 sorption capacity and stability on multicycle operation. *Ind. Eng. Chem. Res.* **2008**, *47*, 9537–9543. [CrossRef]
22. Martavaltzi, C.S.; Lemonidou, A.A. Development of new CaO based sorbent materials for CO_2 removal at high temperature. *Microporous Mesoporous Mater.* **2008**, *110*, 119–127. [CrossRef]
23. Florin, N.H.; Fennell, P. Synthetic CaO-based sorbent for CO_2 capture. *Energy Procedia* **2011**, *4*, 830–838. [CrossRef]
24. Stendardo, S.; Andersen, L.K.; Herce, C. Self-activation and effect of regeneration conditions in CO_2-carbonate looping with $CaO\text{-}Ca_{12}Al_{14}O_{33}$ sorbent. *Chem. Eng. J.* **2013**, *220*, 383–394. [CrossRef]
25. Lu, H.; Reddy, E.P.; Smirniotis, P.G. Calcium oxide based sorbents for capture of carbon dioxide at high temperatures. *Ind. Eng. Chem. Res.* **2006**, *45*, 3944–3949. [CrossRef]
26. Liu, W.G.; Low, N.W.L.; Feng, B.; Wang, G.; Costa, J.C. Calcium precursors for the production of CaO sorbents for multicycle CO_2 capture. *Environ. Sci. Technol.* **2010**, *44*, 841–847. [CrossRef] [PubMed]

27. Wang, Y.; Memon, M.Z.; Seelro, M.A.; Fu, W.; Gao, Y.; Dong, Y.; Ji, G. A review of CO_2 sorbents for promoting hydrogen production in the sorption-enhanced steam reforming process. *Int. J. Hydrogen Energy* **2021**, *46*, 23358–23379. [CrossRef]
28. Di Giuliano, A.; Gallucci, K.; Foscolo, P.U.; Courson, C. Effect of Ni precursor salts on Ni mayenite catalysts for steam methane reforming and on Ni CaO mayenite materials for sorption enhanced steam methane reforming. *Int. J. Hydrogen Energy* **2019**, *44*, 6461–6480. [CrossRef]
29. Clough, P.T.; Boot-Handford, M.E.; Zheng, L.; Zhang, Z.; Fennell, P.S. Hydrogen Production by Sorption Enhanced Steam Reforming (SESR) of Biomass in a Fluidised-Bed Reactor Using Combined Multifunctional Particles. *Materials* **2018**, *11*, 859–882. [CrossRef]
30. Langford, J.I.; Wilson, A.J.C. Scherrer after sixty years: A survey and some new results in the determination of crystallite size. *J. Appl. Crystallogr.* **1978**, *11*, 102–113. [CrossRef]
31. Rapagnà, S.; Virginie, M.; Gallucci, K.; Courson, C.; Di Marcello, M.; Kiennemann, A.; Foscolo, P.U. Fe/olivine catalyst for biomass steam gasification: Preparation, characterization and testing at real process conditions. *Catal. Today* **2011**, *176*, 163–168. [CrossRef]
32. Brown, M.D.; Baker, E.G.; Mudge, L.K. Environmental design considerations for thermochemical biomass energy. *Biomass* **1986**, *11*, 255–270. [CrossRef]
33. Micheli, F.; Sciarra, M.; Courson, C.; Gallucci, K. Catalytic steam methane reforming enhanced by CO_2 capture on CaO based bi-functional compounds. *J. Energy Chem.* **2017**, *26*, 1014–1025. [CrossRef]
34. Di Giuliano, A.; Giancaterino, F.; Courson, C.; Foscolo, P.U.; Gallucci, K. Development of a Ni-CaO-mayenite combined sorbent-catalyst material for multicycle sorption enhanced steam methane reforming. *Fuel* **2018**, *234*, 687–699. [CrossRef]
35. Rapagnà, S.; Jand, N.; Kiennemann, A.; Foscolo, P.U. Steam-gasification of biomass in a fluidised-bed of olivine particles. *Biomass Bioenergy* **2000**, *19*, 187–197. [CrossRef]
36. Chen, G.H. Mechanical activation of calcium aluminate formation from $CaCO_3$-Al_2O_3 mixtures. *J. Alloys Compd.* **2006**, *416*, 279–283. [CrossRef]
37. Chatterjee, A.K.; Zhmoidin, G.I. The phase equilibrium diagram of the system CaO-Al_2O_3-CaF_2. *J. Mater. Sci.* **1972**, *7*, 93–97. [CrossRef]
38. Janek, J.; Lee, D.K. Defect chemistry of the mixed conducting cage compound $Ca_{12}Al_{14}O_{33}$. *J. Korean Ceram. Soc.* **2010**, *47*, 99–105. [CrossRef]
39. Salhi, N.; Boulahouache, A.; Petit, C.; Kiennemann, A.; Rabia, C. Steam reforming of methane to syngas over $NiAl_2O_4$ spinel catalysts. *Int J Hydrogen Energy* **2011**, *36*, 11433–11439. [CrossRef]
40. Bhatia, S.K.; Perlmutter, D.D. A random pore model for fluid-solid reactions. I: Isothermal, kinetic control. *AICHE J.* **1980**, *26*, 379–386. [CrossRef]
41. Martavaltzi, C.S.; Lemonidou, A.A. Hydrogen production via sorption enhanced reforming of methane: Development of a novel hybrid material-reforming catalyst and CO_2 sorbent. *Chem. Eng. Sci.* **2010**, *65*, 4134–4140. [CrossRef]
42. Di Giuliano, A.; Girr, J.; Massacesi, R.; Gallucci, K.; Courson, C. Sorption enhanced steam methane reforming by Ni–CaO materials supported on mayenite. *Int. J. Hydrogen Energy* **2017**, *42*, 13661–13680. [CrossRef]
43. Radfarnia, H.R.; Iliuta, M.C. Development of Al-stabilized CaO-nickel hybrid sorbent-catalyst for sorption-enhanced steam methane reforming. *Chem. Eng. Sci.* **2014**, *109*, 212–219. [CrossRef]
44. Kim, J.N.; Ko, C.H.; Yi, K.B. Sorption enhanced hydrogen production using one-body CaO-$Ca_{12}Al_{14}O_{33}$-Ni composite as catalytic absorbent. *Int. J. Hydrogen Energy* **2013**, *38*, 6072–6078. [CrossRef]
45. Virginie, M.; Courson, C.; Niznansky, D.; Chaoui, N.; Kiennemann, A. Characterization and reactivity in toluene reforming of a Fe/olivine catalyst designed for gas cleanup in biomass gasification. *Appl. Catal. B.* **2010**, *101*, 90–100. [CrossRef]
46. Li, C.; Hirabayashi, D.; Suzuki, K. A crucial role of O^{2-} and O_2^{2-} on mayenite structure for biomass tar steam reforming over Ni/$Ca_{12}Al_{14}O_{33}$. *Appl. Catal. B.* **2009**, *88*, 351–360. [CrossRef]
47. Pecharaumporn, P.; Wongsakulphasatch, S.; Glinrun, T.; Maneedaeng, A.; Hassan, Z.; Assabumrungrat, S. Synthetic CaO-based sorbent for high-temperature CO_2 capture in sorption-enhanced hydrogen production. *Int. J. Hydrogen Energy* **2019**, *44*, 20663–20677. [CrossRef]
48. Nimmas, T.; Jamrunroj, P.; Wongsakulphasatch, S.; Kiatkittipong, W.; Laosiripojana, N.; Gong, J.; Assabumrungrat, S. Influence of CaO precursor on CO2 capture performance and sorption-enhanced steam ethanol reforming. *Int. J. Hydrogen Energy* **2019**, *44*, 20649–20662. [CrossRef]
49. Iftekhar, S.; Grins, J.; Svensson, G.; Lööf, J.; Jarmar, T.; Botton, G.A. Phase formation of $CaAl_2O_4$ from $CaCO_3$-Al_2O_3 powder mixtures. *J. Eur. Ceram. Soc.* **2008**, *28*, 747–756. [CrossRef]